Complete Assignment of ^{13}C NMR Spectra and Determination of Orientational Order Parameter for Antiferroelectric Liquid-Crystalline MHPOBC

Toshihito Nakai,[†,‡] Hiroki Fujimori,[†,§] Daisuke Kuwahara,[†] and Seiichi Miyajima*[,†]

Institute for Molecular Science, Myodaiji, Okazaki 444-8585, Japan, Department of Biotechnology, Tokyo University of Agriculture and Technology, Koganei 184-8588, Japan, and College of Humanities and Sciences, Nihon University, Sakurajosui, Setagaya-ku, Tokyo 156-8550, Japan

Received: July 13, 1998; In Final Form: October 14, 1998

Complete assignment of the ^{13}C NMR lines is reported for both isotropic and oriented samples of antiferroelectric liquid-crystalline MHPOBC. Two-dimensional double-quantum coherence spectroscopy (2-D INADEQUATE) in the isotropic phase and field alignment-induced shifts (AIS) were studied. $^{19}F-^{13}C$ dipolar quartets were measured for TFMHPOBC, where a methyl group attached to the chiral center of MHPOBC is replaced by a trifluoromethyl group, to assist the assignment. Shielding tensor principal elements were determined for each carbon by site-separated spinning sideband spectroscopy (2-D TOSS-deTOSS). The orientational order parameter has been evaluated to be 0.73 at 403 K in the S_A phase using the experimentally determined AIS and the tensor elements and assuming an intramolecular free rotation model.

I. Introduction

^{13}C nuclear magnetic resonance (NMR) is a powerful method in analyzing orientational orders and molecular motions in liquid crystals because it probes every possible detail of intramolecular information from the site-separated chemical-shift spectra. In the liquid-crystalline state, molecules often align along the magnetic field because of the anisotropy in diamagnetic susceptibility. This causes alignment-induced shifts (AIS) on the ^{13}C NMR spectra. By analyzing AIS with theoretical models, one can obtain details of the intramolecular orders and motions, as well as the orientational order of a molecule as a whole. Assignment of the spectral lines is, therefore, an inevitable task to this goal. However, the assignment of the field-aligned spectra is generally difficult because the transition from the isotropic to the liquid-crystal phases is first order, which means AIS suddenly appears at the phase transition and one cannot follow the lines even if the line assignment is complete in the isotropic liquid state. This difficulty may restrict the use of ^{13}C NMR when we start the NMR study on the microscopic origin of antiferroelectricity.

This paper reports complete assignment of the field-aligned as well as the isotropic ^{13}C NMR spectra of MHPOBC and its analogue TFMHPOBC. MHPOBC, 4-[(1-methylheptyloxy)-carbonyl]phenyl 4-[(4-(octyloxy)biphenyl]carboxylate, is a prototypical compound for which antiferroelectricity was confirmed.[1,2] Figure 1 shows the molecular structure and the numbering (j) scheme of the carbon atoms. TFMHPOBC is a derivative where the methyl group numbered as $j = 30$ of MHPOBC is replaced by a trifluoromethyl group and also exhibits an antiferroelectric liquid-crystalline phase.[3] Spectral assignment for the chain parts ($j = 1-8$ and $23-30$) is reported in our previous paper.[4] This paper describes the assignment for the core part ($j = 9-22$) and completes the assignment. As a first application of the assignment, the location of the molecular long axis and the value of the orientational order parameter are determined.

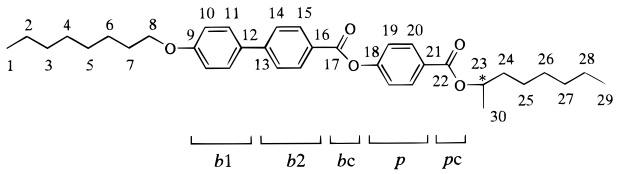

Figure 1. Molecular structures of MHPOBC and TFMHPOBC. The carbon atom numbered as $j = 23$, indicated by an asterisk (∗), is the chiral center. The methyl group with the $j = 30$ carbon for MHPOBC is replaced by a trifluoromethyl group for TFMHPOBC. Intramolecular fragments are also indicated.

II. Experimental Section

The sample of *R*-MHPOBC with high optical purity was provided by Showa Shell Petroleum Co. through Prof. A. Fukuda and used without further purification. The phase sequence and the transition temperatures have been reported with adiabatic calorimetry.[5] The isotropic liquid (I) phase transforms to liquid-crystalline phases with successive phase transitions, I (421.73 K) → smectic A (S_A) (396.51 K) → smectic Cα* ($S_{C\alpha}$*) (395.29 K) → ferroelectric smectic C* (S_C*) (393.64 K) → ferrielectric smectic Cγ* ($S_{C\gamma}$*) (392.84 K) → antiferroelectric smectic C* (S_{CA}*), and finally crystallizes.

Two-dimensional double-quantum coherence spectra (2-D INADEQUATE)[6] were taken using a Bruker DSX-400 spectrometer working at 100.63 MHz for ^{13}C. The sample was heated to the isotropic phase (424 K), and the measurement was made under magic-angle spinning (MAS) at 1.00 kHz for better spectral resolution. In all the experimental spectra, the shielding constants are expressed in parts per million from tetramethylsilane (TMS) with higher values for higher resonance frequencies.

Field-aligned spectra in the liquid-crystalline states of MHPOBC and TFMHPOBC were taken with a JEOL GSX-270

[†] Institute for Molecular Science.
[‡] Tokyo University of Agriculture and Technology.
[§] Nihon University.

10.1021/jp982996u CCC: $18.00
Published on Web 01/05/1999

spectrometer working at 67.94 MHz. Continuous-wave proton decoupling was applied. Usually, cross polarization with a contact time of 1 ms was applied for signal enhancement. Because of the intense decoupling field of typically 50 kHz, an interval as long as 6 s was inserted to avoid sample heating. The sample was evacuated for more than 10 h and sealed in a 5 mm ϕ Pyrex tube after a freeze−pump−thaw cycle to remove humidity and oxygen. The sample was then fixed tightly in the probehead.

Detailed experiments on the temperature dependence for the field-aligned sample were conducted with the Bruker DSX-400 spectrometer and a wide-line probehead to allow better control of the temperature.

Two-dimensional site-separated spinning sideband spectroscopy (2-D TOSS-deTOSS)[7] with spinning frequency of 3.000 kHz was conducted with the DSX-400 spectrometer.

III. Theory of NMR Shielding Spectrum for Oriented Liquid Crystals

When a liquid crystal is aligned in the magnetic field, the observed shielding constant for the individual carbon nucleus numbered as j is a motional average of the projection of the individual shielding tensor onto the z-axis of the laboratory frame (LAB) where z^{LAB} is taken along the external field. The projection is calculated using a spherical tensor $\sigma^{j-\mathrm{PAS}}(j)$ defined on the jth shielding principal axis system (j-PAS) and Wigner rotation matrix $D^{(2)}_{m0}(j\text{-PAS} \rightarrow \mathrm{LAB})$, such that[8]

$$\langle\sigma^{\mathrm{LAB}}_{zz}(j)\rangle = -\frac{1}{\sqrt{3}}\sigma^{j-\mathrm{PAS}}_{00}(j) + \sqrt{\frac{2}{3}}\sum_{m=-2}^{2}\sigma^{j-\mathrm{PAS}}_{2m}(j)\langle D^{(2)}_{m0}(j\text{-PAS} \rightarrow \mathrm{LAB})\rangle \quad (1)$$

The spherical tensor is related with the Cartesian shielding tensor by formal relationships

$$\sigma^{j-\mathrm{PAS}}_{00}(j) = -\frac{1}{\sqrt{3}}\,\mathrm{tr}\sigma(j) = -\sqrt{3}\sigma_{\mathrm{iso}}(j) \quad (2)$$

$$\sigma^{j-\mathrm{PAS}}_{20}(j) = \sqrt{\frac{3}{2}}\,[\sigma^{j-\mathrm{PAS}}_{zz}(j) - \sigma^{j-\mathrm{PAS}}_{\mathrm{iso}}(j)] \quad (3)$$

$$\sigma^{j-\mathrm{PAS}}_{2\pm1}(j) = 0 \quad (4)$$

and

$$\sigma^{j-\mathrm{PAS}}_{2\pm2}(j) = \frac{1}{2}[\sigma^{j-\mathrm{PAS}}_{xx}(j) - \sigma^{j-\mathrm{PAS}}_{yy}(j)] \quad (5)$$

where the Cartesian tensor elements are defined so that

$$\sigma^{j-\mathrm{PAS}}_{xx}(j) \geq \sigma^{j-\mathrm{PAS}}_{yy}(j) \geq \sigma^{j-\mathrm{PAS}}_{zz}(j) \quad (6)$$

and the average, $\sigma_{\mathrm{iso}}(j)$, is called the isotropic shielding constant.

The quantity $\langle D^{(2)}_{m0}(j\text{-PAS} \rightarrow \mathrm{LAB})\rangle$ contains the geometrical location of the j-PAS axes within a molecule and all the information on molecular motions. The j-PAS → LAB transformation is divided into five steps in our theoretical model by introducing additional four coordinate systems as described in Figure 2. The fragment system (f-FRAG) is defined on a rigid intramolecular fragment on which any motional freedoms are neglected. The core part of MHPOBC may be divided into five fragments indexed as $f = b1, b2, p, bc$, and pc, as indicated in

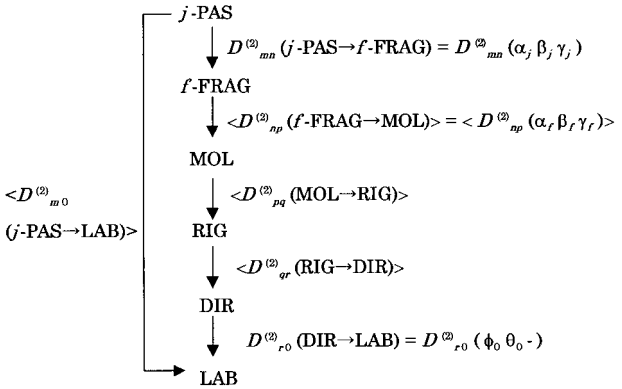

Figure 2. Coordinate transformations and the corresponding Wigner rotation matrixes and Eulerian angles.

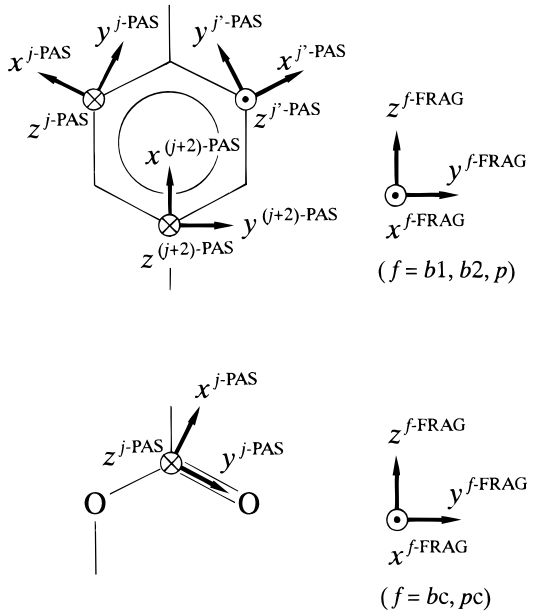

Figure 3. Orientations of the shielding principal axes for each carbon with relative geometrical relationships with the fragment coordinate systems.

Figure 1. The $b1$-, $b2$-, and p-FRAG represent aromatic-ring fragments of the biphenylene first ring (which contains j = 9−12), biphenylene second ring (j = 13−16), and phenylene ring (j = 18−21), respectively. bc and pc represent carbonyl-group fragments attached to biphenylene and phenylene groups, respectively. The coordinate axes for f-FRAG are taken along the axes of mechanical moments of inertia in the order

$$I^{f-\mathrm{FRAG}}_{xx}(j) \geq I^{f-\mathrm{FRAG}}_{yy}(j) \geq I^{f-\mathrm{FRAG}}_{zz}(j) \quad (7)$$

and are illustrated in Figure 3 together with typical relative relationships with j-PAS axes. For all the carbon atoms under the present investigation, the most shielding axis ($z^{j-\mathrm{PAS}}$) lies along $x^{f-\mathrm{FRAG}}$, and this means the second Eulerian angles β_j for j-PAS → f-FRAG transformation are always $\pi/2$. Typical values for the shielding principal components and Eulerian angles are tentatively taken from the literature[9] and listed in Table 1; the shielding components will be refined in section V.1 on the basis of our experiment. The angles α_j and γ_j take almost definite values for aromatic carbons but are somewhat uncertain for carbonyl carbons: $y^{bc-\mathrm{FRAG}}$ or $y^{pc-\mathrm{FRAG}}$ axes point nearly parallel to the C═O bond but sometimes deviate from the bond direction, depending on the electronic structure of the ester linkages.

The $\sigma^{f-\mathrm{FRAG}}_{zn}$ is then transformed to the molecular system (MOL) where the three coordinates are defined along the three

TABLE 1: Typical Shielding Tensor Components and the Eulerian Angles for *j*-PAS → *f*-FRAG Transformations[a]

types of carbon atoms	$\sigma_{xx}^{j-\mathrm{PAS}}$ (ppm)	$\sigma_{yy}^{j-\mathrm{PAS}}$ (ppm)	$\sigma_{zz}^{j-\mathrm{PAS}}$ (ppm)	σ_{iso} (ppm)	α_j (rad)	β_j (rad)	γ_j (rad)	$\mathrm{AIS}_0^{\mathrm{free}}$ (ppm)
aromatic protonated carbons	215	145	17	126	$\pi/3$	$\pi/2$	$0, \pi$	37
aromatic nonprotonated carbons	221	160	21	134	0	$\pi/2$	0	87
ester carbonyl carbons	258	132	107	166	$\pi/6$	$\pi/2$	0	61

[a] Alignment-induced shifts ($\mathrm{AIS}_0^{\mathrm{free}}$) are also shown in ppm from TMS. $\mathrm{AIS}_0^{\mathrm{free}}$ are estimated for the free internal rotation model with $S_{00} = 1$, $\beta_f = 0$, and $\theta_0 = 0$.

principal axes of the moment of inertia of the whole molecule. The second transformation is described by Eulerian angles α_f, β_f, and γ_f. Since the three fragments, *b*1, *b*2, and *bc*, belonging to the biphenylene core have the common $z^{b-\mathrm{FRAG}}$ axis, the angles β_f are unique, i.e., $\beta_b = \beta_{b1} = \beta_{b2} = \beta_{bc}$. A similar relationship, $\beta_p = \beta_{pc}$, holds for the phenylene core. Therefore, the terms biphenylene core and phenylene core are used for the groups of fragments which have the respective common $z^{f-\mathrm{FRAG}}$ axes, and these axes may be called the "core axes." The difference in α_f within each core such as $|\alpha_{b1} - \alpha_{b2}|$ describes the dihedral angle between the fragments, and the possible time dependence of α_f describes the rotation of the fragment about $z^{f-\mathrm{FRAG}}$.

The shielding tensor projected on MOL is then averaged by rotation of a molecule about the long molecular axis, z^{MOL}. This process is described by an average Wigner rotation matrix $\langle D_{pq}^{(2)}(\mathrm{MOL} \rightarrow \mathrm{RIG})\rangle$ which characterizes the extent of molecular biaxiality or asymmetry of the molecular rotation. The resultant system RIG, the system of the molecule as a rigid body,[4] is then transformed to DIR, the director frame. This process describes the orientational order of the molecule as a whole. The well-known Maier-Saupe's orientational order parameter[10] S_{00} is defined as the zero−zero component of this averaged matrix such that

$$S_{00} \equiv \langle D_{00}^{(2)}(\mathrm{RIG} \rightarrow \mathrm{DIR})\rangle \tag{8}$$

The last transformation is the one from DIR frame to the laboratory frame which contains the polar angle, θ_0, and the azimuthal angle ϕ_0 between x^{DIR} and x^{LAB}, the latter of which is related to possible phase biaxiality.

Each of the Wigner matrixes in Figure 2 is related to the respective degree of freedom. If we assume that the motional modes are not coupled with one another,[11] eq 1 is rewritten as

$$\langle \sigma_{zz}^{\mathrm{LAB}}(j)\rangle = \sigma_{\mathrm{iso}}(j) + \sqrt{\frac{2}{3}} \sum_{r=-2}^{2} \sum_{q=-2}^{2} \sum_{p=-2}^{2} \sum_{n=-2}^{2} \sum_{m=-2}^{2} \sigma_{2m}^{j-\mathrm{PAS}}(j) D_{mn}^{(2)}(j\text{-PAS} \rightarrow f\text{-FRAG}) \times \langle D_{np}^{(2)}(f\text{-FRAG} \rightarrow \mathrm{MOL})\rangle \langle D_{pq}^{(2)}(\mathrm{MOL} \rightarrow \mathrm{RIG})\rangle \times \langle D_{qr}^{(2)}(\mathrm{RIG} \rightarrow \mathrm{DIR})\rangle D_{r0}^{(2)}(\mathrm{DIR} \rightarrow \mathrm{LAB}) \tag{9}$$

where the brackets $\langle\ \rangle$ represent averages by the respective motional modes: $\langle D_{np}^{(2)}(f\text{-FRAG} \rightarrow \mathrm{MOL})\rangle$, $\langle D_{pq}^{(2)}(\mathrm{MOL} \rightarrow \mathrm{RIG})\rangle$, and $\langle D_{qr}^{(2)}(\mathrm{RIG} \rightarrow \mathrm{DIR})\rangle$ describe, respectively, the intramolecular fragmental motion, uniaxial rotation of the molecule as a whole about the long molecular axis, and the fluctuation of the molecular long axis about the director. In the present paper, we do not dig into the molecular biaxiality and phase biaxiality because the present purposes are (i) spectral assignment and (ii) determination of S_{00} in the S_A phase. If we neglect the biaxialities, then

$$\langle D_{pq}^{(2)}(\mathrm{MOL} \rightarrow \mathrm{RIG})\rangle = \delta_{p0}\delta_{q0} \tag{10}$$

and

$$\langle D_{qr}^{(2)}(\mathrm{RIG} \rightarrow \mathrm{DIR})\rangle = \delta_{q0}\delta_{r0}S_{00} \tag{11}$$

follows and eq 9 reduces to

$$\langle \sigma_{zz}^{\mathrm{LAB}}(j)\rangle = \sigma_{\mathrm{iso}}(j) + \sqrt{\frac{2}{3}} \sum_{n=-2}^{2} \sum_{m=-2}^{2} \sigma_{2m}^{j-\mathrm{PAS}}(j) D_{mn}^{(2)}(j\text{-PAS} \rightarrow f\text{-FRAG}) \times \langle D_{n0}^{(2)}(f\text{-FRAG} \rightarrow \mathrm{MOL})\rangle S_{00} D_{00}^{(2)}(\mathrm{DIR} \rightarrow \mathrm{LAB}) = \sigma_{\mathrm{iso}}(j) + \sqrt{\frac{2}{3}} \sum_{n=-2}^{2} \sum_{m=-2}^{2} \sigma_{2m}^{j-\mathrm{PAS}}(j) D_{mn}^{(2)}(\alpha_j,\beta_j,\gamma_j) \times \langle D_{n0}^{(2)}(\alpha_f\beta_f\gamma_f)\rangle S_{00} P_2(\cos\theta_0) \tag{12}$$

Here P_2 is the Legendre polynomial of rank two, namely

$$P_2(\cos\theta_0) = \frac{1}{2}(3\cos^2\theta_0 - 1) \tag{13}$$

Remembering $\beta_j = \pi/2$ holds for every carbon under study, eq 10 is fairly simplified and expressed in a Cartesian tensor form, as

$$\langle \sigma_{zz}^{\mathrm{LAB}}(j)\rangle = \sigma_{\mathrm{iso}}(j) + \tfrac{1}{2}[\sigma_{zz}^{j-\mathrm{PAS}}(j) - \sigma_{\mathrm{iso}}(j)] \times \left[-P_2(\cos\beta_f) + \tfrac{3}{2}\langle\cos 2(\gamma_j + \alpha_f)\rangle \sin^2\beta_f\right] S_{00} P_2(\cos\theta_0) + \tfrac{1}{2}[\sigma_{xx}^{j-\mathrm{PAS}}(j) - \sigma_{yy}^{j-\mathrm{PAS}}(j)] \times \left[\cos 2\alpha_j P_2(\cos\beta_f) - \sin 2\alpha_j \langle\sin(\gamma_j + \alpha_f)\rangle \sin 2\beta_f + \tfrac{1}{2}\cos 2\alpha_j \langle\cos 2(\gamma_j + \alpha_f)\rangle \sin^2\beta_f\right] S_{00} P_2(\cos\theta_0) \tag{14}$$

Here we assumed that averaging over intramolecular motions is made through the time dependence of α_f while β_f are fixed, since we dealt with intramolecular uniaxial rotations about $z^{f-\mathrm{FRAG}}$.

We first intend to apply eq 14 to the assignment of the oriented liquid-crystal spectra, and so a rather rough approximation is made, which is to assume "free" rotation of each fragment about $z^{f-\mathrm{FRAG}}$. The term free means that the rotational potential has symmetry higher than C_3 and/or, accordingly, that the rotational motions among the neighboring fragments are uncorrelated. Then all the braced quantities $\langle\ \rangle$ on the right-hand side of eq 14 become zero to give

$$\langle \sigma_{zz}^{\mathrm{LAB}}(j)\rangle^{\mathrm{free}} = \sigma_{\mathrm{iso}}(j) + \left\{-\frac{1}{2}[\sigma_{zz}^{j-\mathrm{PAS}}(j) - \sigma_{\mathrm{iso}}(j)] + \frac{1}{2}[\sigma_{xx}^{j-\mathrm{PAS}}(j) - \sigma_{yy}^{j-\mathrm{PAS}}(j)]\cos 2\alpha_j\right\} P_2(\cos\beta_f) S_{00} P_2(\cos\theta_0) \tag{15}$$

A more rigorous expression, eq 14, will be used in section V.

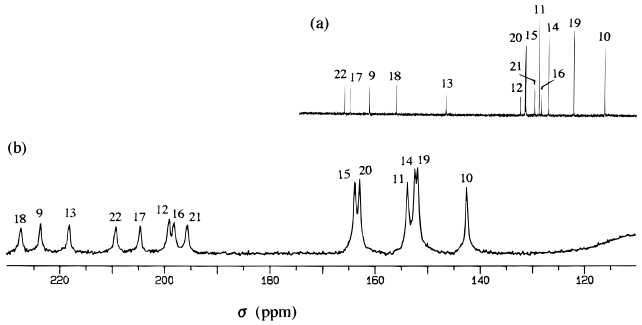

Figure 4. ^{1}H-decoupled ^{13}C NMR spectra of MHPOBC in the (a) I phase with MAS and (b) the S_A phase at 403 K with field-aligned conditions.

IV. Spectral Assignment

IV.1. Isotropic Spectrum. MHPOBC has 14 inequivalent carbon atoms in the core, 12 aromatic and 2 carbonyl, and they appear between 110 and 170 ppm in the isotropic spectrum as shown in Figure 4a. Doubly intense lines coming from the protonated aromatic carbons are easily distinguished from the nonprotonated carbons with single intensity. However, full assignment is difficult with the one-dimensional spectrum. Figure 5a shows the 2-D INADEQUATE spectrum taken in the isotropic phase. Figure 5b is an expanded plot. In either figure, the horizontal axis (f_2) shows chemical shifts expressed in ppm. On the top in each figure is shown the 1-D spectrum for reference. Here the 14 lines are numbered as A−N from the high-frequency side. Generally, 2-D INADEQUATE cross-peaks are found for the neighboring ^{13}C−^{13}C pairs that are coupled with hyperfine-mediated indirect (J) coupling and each cross-peak consists of two spots separated by $J(^{13}\text{C}-^{13}\text{C})$.[6] One can, therefore, trace the nearest-neighbor connections. From Figure 5 three groups of connections, A−I−G−M−D, C−N−J−F, and E−L−H−K, are easily detected while the connection with line B is missing. In the core part to MHPOBC, the ^{13}C−^{13}C connections may be grouped into two groups, namely, 9 carbons for $j = 9-17$ and 5 carbons for $j = 18-22$. Therefore, two of the individual ^{13}C−^{13}C connections are missing in our experiment; at least one of them is related to line B. To find out the connections with subtle intensity, the vertical axis (f_1) spectrum was employed. The f_1 spectrum, in Hertz, consists of peaks at sum frequencies of the J-coupled pairs relative to the carrier frequency, and assignments are shown in Figure 5b. We found a peak at −409 Hz with significant intensity that was undetectable in the 2-D contour plot. The detected frequency was found to correspond to the sum of the f_1 frequencies of E and F. Considering that lines B and C appear in the carbonyl and the oxo−carbon regions, respectively, in the 1-D spectrum, the longer ^{13}C−^{13}C connection chain is constructed as C−N−J−F−E−L−H−K···B and is assigned to $j = 9-10-11-12-13-14-15-16\cdots17$. The shorter chain A−I−G−M−D is assigned to $j = 22-21-20-19$.

Our effort to find the connection K···B was unsuccessful, probably because the spin−lattice relaxation rates are slow for both carbons and also because the magnitude of J ($j = 16-17$) does not match the pulse intervals that were optimized for aromatic carbon pairs in the present experiment.[12] Though the connection is not thorough, the assignment accomplished here and shown in Figure 4a is fully acceptable from knowledge of the literature:[13] Two carbonyl carbons, A and B, are very closely located, but the known spectral data indicate that the ester carbonyl carbon attached to oxo−aromatic groups usually appears on the lower frequency side (by 1−3 ppm) than the one attached to oxo−aliphatic groups.

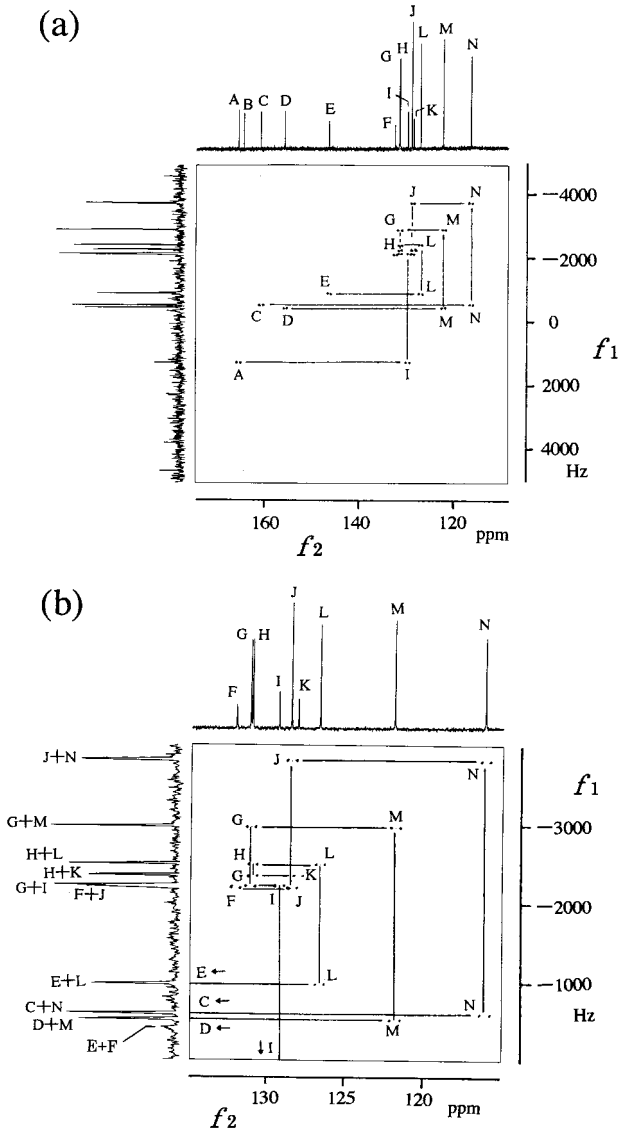

Figure 5. 2-D INADEQUATE spectrum of MHPOBC in the I phase. (b) Expanded version of a.

IV.2. Oriented Spectrum: Temperature Dependence. Figure 4b shows the ^{13}C NMR spectrum in the S_A phase of oriented MHPOBC at 403 K. The purpose of this and the following two sections is to assign the oriented spectrum. Difficulty lies in that the assignment for the isotropic spectrum is not enough for this purpose because the AIS (which is the difference between spectra b and a) suddenly appears at the I/S_A first-order phase transition and their magnitudes are different depending on the carbon sites. However, a rough assignment is possible using the results of the isotropic spectrum and referring to the results of theoretical section III. If we make a simple approximation of free rotation of the fragment, eq 15 simplifies to

$$\text{AIS}(j)^{\text{free}} = \left\{-\frac{1}{2}[\sigma_{zz}^{j-\text{PAS}}(j) - \sigma_{\text{iso}}(j)] + \frac{1}{2}[\sigma_{xx}^{j-\text{PAS}}(j) - \sigma_{yy}^{j-\text{PAS}}(j)]\cos 2\alpha_j\right\} P_2(\cos\beta_f) S_{00} P_2(\cos\theta_0) \quad (16)$$

The quantities in the square brackets may be estimated by the shielding tensor elements obtained by the solid-state NMR studies, and the details are described for MHPOBC in section V. Here we take a rough approach for the spectral assignment

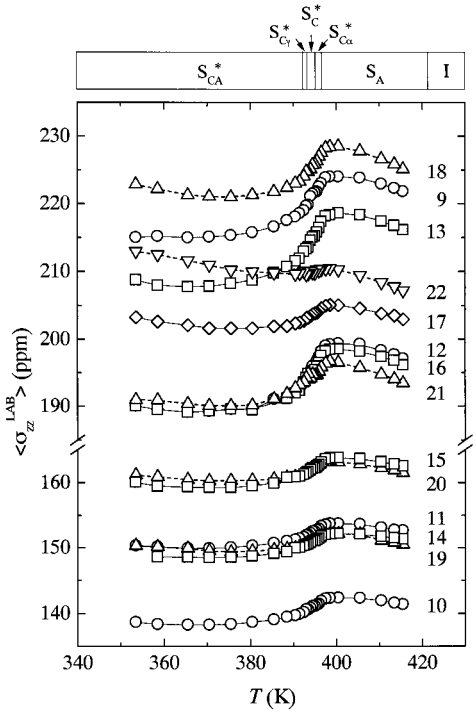

Figure 6. Temperature dependence of the shielding constants for oriented MHPOBC in the liquid-crystalline phases. Phase transition temperatures are indicated in the figure. The symbols indicate the fragments: (○) *b*1, (□) *b*2, (◇) *bc*, (△) *p*, and (▽) *pc*. Solid and dashed curves are drawn for biphenylene and phenylene cores, respectively.

using literature data for well-known compounds. Table 1 summarizes the typical tensor elements for three different types of carbon atoms.[9] By applying eq 16, on the condition that $S_{00} = 1$, $\beta_f = 0$, and $\theta_0 = 0$, one obtains the magnitudes of AIS_0^{free} as listed in Table 1. The three different types of carbons exhibit characteristically different values, and so this estimate can be a great help for the assignment. Thus, the six lines in the low-frequency region in Figure 4b with less AIS are assigned to the aromatic protonated carbons and the rest of the peaks to nonprotonated aromatic and carbonyl carbons. A significant difference in AIS_0^{free} between aromatic protonated and nonprotonated carbons comes mainly from the difference in α_j. The second shielding components σ_{yy}^{j-PAS} contribute in the oriented spectrum of protonated carbons, while they do not in the case of nonprotonated carbons.

The next problem was to distinguish the lines belonging to biphenylene and phenylene cores. We resorted to the analysis of the temperature (T) dependence. Figure 6 shows the experimentally obtained $\langle\sigma_{zz}^{LAB}(j)\rangle$ as a function of T. Fortunately, we found that discontinuities in $\langle\sigma_{zz}^{LAB}(j)\rangle$ are very small on crossing the successive phase transitions, $S_A-S_{C\alpha}^*-S_C^*-S_{C\gamma}^*-S_{CA}^*$, on lowering the temperature, and therefore, the lines could be traced across the transitions. Considering that the T dependence of $\langle\sigma_{zz}^{LAB}(j)\rangle$ comes from $S_{00}P_2(\cos\theta_0)$ from eq 15 and that S_{00} is not very dependent on T in the smectic phases, especially at low temperature, the significant change (decrease) in $\langle\sigma_{zz}^{LAB}(j)\rangle$ in the phase-transition region comes from the T-dependent change in θ_0. Since the quantity in { } in eq 15 is negative and $P_2(\cos\beta_f)S_{00}$ is positive, the continuous decrease in AIS(j) means a continuous increase in θ_0. This is explained by the gradual increase in tilt angle θ_t between the smectic layer normal and the director, as reported by Blinc et al. for DOBAMBC.[14] This finding proves that z^{DIR} makes an angle θ_t from z^{LAB} and, therefore, $\theta_0 = \theta_t$ in all phases, except S_A, of *R*-MHPOBC.

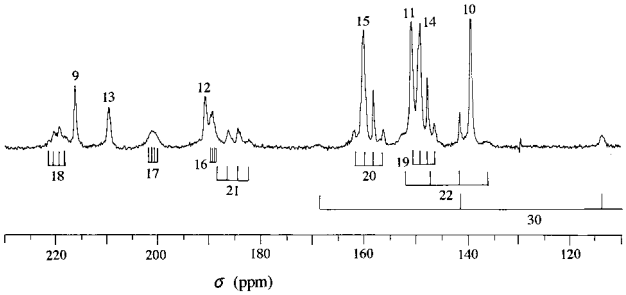

Figure 7. ^{1}H-decoupled ^{13}C NMR spectrum of TFMHPOBC in the S_A phase (393 K) with field-aligned conditions. The assigned $^{13}C-^{19}F$ dipolar quartets are indicated.

The above quantity $S_{00}P_2(\cos\theta_0)$ is the one determined for the molecular assembly and does not depend on the specific site (j) within a molecule. Equations 15 and 16 indicate that both AIS(j) and their widths with a T-dependent change in $\langle\sigma_{zz}^{LAB}(j)\rangle$ are proportional to { } $P_2(\cos\beta_f)$, where { } reflects what type of carbon (protonated, aromatic nonprotonated, or carbonyl) the jth carbon is and $P_2(\cos\beta_f)$ depends on which core (biphenylene core with $\beta_f = \beta_b$ or phenylene core with $\beta_f = \beta_b$) it belongs to. Therefore, the former assignment of the six lower frequency lines to aromatic protonated carbons has been confirmed; namely, less AIS(j) and less T dependence are characteristic of this type of carbons. Among the rest of the lines appearing at 190−230 ppm, the two lines at 200−210 ppm were assigned to carbonyl carbons because of less pronounced T dependence and the remaining six to aromatic nonprotonated carbons.

Careful examination reveals that two of the six lines in each of the protonated and nonprotonated aromatic lines exhibit a less pronounced T dependence, indicated by dashed lines in Figure 6, namely, $j = 19$, 20 and $j = 18$, 21, respectively. It is noted also that $\langle\sigma_{zz}^{LAB}(j)\rangle$ of these lines tend to increase again at the lowest temperature region of the S_{CA}^* phase. These lines are assigned to the carbons belonging to the phenylene core. Actually the slightly different behaviors of the carbons belonging to biphenylene and phenylene cores are related partly to molecular biaxiality and phase biaxiality, which are neglected in the theoretical treatment of this paper and will be treated in the subsequent paper. For assignment purposes, here we will not mention any more about the biaxiality problem.

The present assignment was confirmed by examining the CP efficiencies: The lines belonging to the phenylene core were less intense than the corresponding lines of the biphenylene core, in the S_A phase.

How to assign the four ($f = b1$, $b2$) and two ($f = p$) protonated lines ($j = 10$, 11, 14, 15 and $j = 19$, 20), how to assign the four ($f = b1$, $b2$) and two ($f = p$) aromatic nonprotonated lines ($j = 9$, 12, 13, 16 and $j = 18$, 21), and how to discriminate the two carbonyl lines ($j = 17$, 22) are still to be determined at this stage but will be solved below.

IV.3. Oriented Spectrum of TFMHPOBC. The ^{13}C NMR spectrum of TFMHPOBC was recorded to assist and accomplish the assignment of MHPOBC. Figure 7 shows the ^{1}H-decoupled ^{13}C spectrum in the S_A phase of TFMHPOBC. The lines are complex because of $^{13}C-^{19}F$ dipole interactions, but the complexity itself contains useful information. Since dipole interactions are sensitive to the internuclear distances, the magnitudes of $^{13}C-^{19}F$ dipolar quartets are a measure of the distance between the C(30)F_3 group and the respective carbons. On the other hand, the center of gravity of each quartet may not differ so much from the corresponding singlet of MHPOBC

TABLE 2: Assignment for Isotropic and Oriented Spectra for TFMHPOBC[a]

j	$\sigma_{iso}(j)$ (ppm)	$\langle\sigma_{zz}^{LAB}(j)\rangle$ (ppm)	AIS(j) (ppm)	$D_{^{13}C-^{19}F}(j)$ (Hz)
9	160.67	215.9	52.2	
10	115.99	139.1	23.1	
11	128.58	150.6	22.0	
12	131.99	190.2	58.2	
13	146.32	209.3	63.0	
14	126.73	149.3	22.6	
15	131.14	160.4	29.3	
16	127.89	189.2	61.3	
17	164.15	200.8	36.7	
18	156.24	219.8	63.3	76
19	122.30	148.1	25.8	88
20	131.71	158.9	27.2	125
21	127.13	185.0	57.9	136
22	164.54	144	−21	334

[a] Shielding constants and AIS are expressed in ppm. Magnitudes of $^{13}C-^{19}F$ dipole interactions in the oriented spectrum are shown in Hertz.

except for C(22), which is the closest to the CF_3 group. Therefore, the aromatic protonated and nonprotonated carbons may be located at 130−160 and 180−220 ppm, respectively. In the nonprotonated carbon region, C(9), C(12), C(13), and C(16) belonging to the biphenylene core are assigned in the order of increasing line widths. C(18) and C(21) in the phenylene core exhibit resolved quartets with a significantly larger quartet for C(21). A broad peak at 200.8 ppm is assigned to C(17) because the dipole interaction is intermediate between those of C(16) and C(18). This further supports the assignment of the similar line to C(17) in MHPOBC. In the protonated carbon region, the sharp and intense four lines are assigned to the biphenylene C(10), C(11), C(14), and C(15) in the order of increasing line widths. Actually the line widths of the two peaks assigned to C(14) and C(15) are very similar. We referred to the order of the isotropic spectrum. C(19) and C(20) in the phenylene fragment exhibit resolved quartets. Finally, the ester carbon C(22) was located at 144 ppm with a widespread quartet.

The splittings of the $^{13}C-^{19}F$ quartets are summarized in Table 2 with the resultant assignment. Very large splittings of 0.72 and 1.85 kHz were observed for C(23) and C(30) because of the short $^{13}C-^{19}F$ distances, though they are out of the scope of our present interest. The assignment summarized in Figure 7 and Table 2 reveals the AIS(j) amounting to more than 50 ppm (59.3 ppm on the average) for aromatic nonprotonated carbons and less than 30 ppm (25.0 ppm on the average) for protonated carbons. Carbonyl carbon C(17) attached to the biphenylene group exhibits an intermediate value of 36.7 ppm. Another carbonyl carbon C(22) is very unusual; AIS (22) is negative.

IV.4. Assignment of the Oriented Spectrum of MHPOBC. The final assignment was made for MHPOBC by referring to the result for TFMHPOBC given in section IV.3 in addition to the rough estimate of the T-dependent AIS described in section IV.2; namely, the lines within each of the biphenylene and phenylene cores of MHPOBC were assigned in the same order as those of TFMHPOBC. The ester carbonyl carbon C(17) which showed "normal" AIS for TFMHPOBC is also found to behave normal for MHPOBC in both the AIS value and its T dependence. The behavior of the other carbonyl carbon C(22) is different from that in TFMHPOBC: The line position is at the higher frequency side of C(17), and its T dependence is very small in the phase-transition region. The final assignment is shown in Figures 4b and 6 and summarized in Table 3. The average values of AIS(j) are 67.7 ppm for aromatic nonprotonated carbons, 28.0 ppm for aromatic protonated carbons, and

TABLE 3: Assignment for Isotropic and Oriented Spectra for MHPOBC

j	$\sigma_{iso}(j)$ (ppm)	$\langle\sigma_{zz}^{LAB}(j)\rangle$ (ppm)	AIS(j) (ppm)
9	160.59	223.0	62.4
10	116.07	141.9	25.8
11	128.58	153.1	24.5
12	132.15	198.4	66.3
13	146.18	217.5	71.3
14	126.74	151.7	25.0
15	131.07	163.2	32.1
16	128.15	197.4	69.3
17	164.14	203.9	39.8
18	155.49	226.8	71.3
19	121.90	151.2	29.3
20	131.18	162.2	31.0
21	129.38	195.0	65.6
22	165.23	208.6	43.4

41.6 ppm for carbonyl carbons. Since the assignment of the lines belonging to the chains was already reported,[4] we have completed the assignment of all the carbons of MHPOBC and TFMHPOBC. This enables a detailed study on the order and dynamics of these interesting antiferroelectric liquid crystals.

A rough estimate for S_{00} is now possible. Comparison of the estimated AIS_0^{free} (for $S_{00} = 1$ and $\beta_f = 0$) given in Table 1 with eq 16 leads to

$$\frac{AIS^{exptl}(S_{00},\beta_f)}{AIS_0^{free}(1,0)} = P_2(\cos\beta_f)S_{00} \qquad (17)$$

for each of the carbon types. By taking the data at 403 K in the S_A phase for aromatic carbons, one obtains, on average, $P_2(\cos\beta_b)S_{00} = 0.74$ for the biphenylene core and $P_2(\cos\beta_p)S_{00} = 0.78$ for the phenylene core. Similarly, $P_2(\cos\beta_b)S_{00} = 0.66$ and $P_2(\cos\beta_p)S_{00} = 0.71$ are obtained for TFMHPOBC at 393 K in the S_A phase. Along the lines of the approximation here, the difference between the two cores within one molecule comes from the difference in β_f. In either compounds, $\beta_b > \beta_p$ is concluded. However, the difference seems too large and the inequality meaning that z^{b-FRAG} tilts from z^{MOL} more than z^{p-FRAG} is unnatural because the main contribution to the moment of inertia for the whole molecule comes from the biphenylene core. These imply a limitation of the present rough approach that employs literature data for the shielding elements. In section V, we extend this analysis by using the experimentally determined tensor elements for MHPOBC.

V. Orientational Order Parameter and the Related Models of Intramolecular Motions

V.1. Determination of Shielding Tensor Elements. Now that the assignment is done, one can obtain S_{00}, the orientational order parameter of a molecule, and β_b and β_p, the angles which specify the direction of the molecular long axis (z^{MOL}) relative to the two fragmental axes (z^{b-FRAG} and z^{p-FRAG}) using eq 14 and the principal tensor components, $\sigma_{xx}^{j-PAS}(j)$, $\sigma_{yy}^{j-PAS}(j)$, and $\sigma_{zz}^{j-PAS}(j)$, for each carbon atom of MHPOBC.

If all the carbon atoms experience the same local field, i.e., they are chemically equivalent or the number of inequivalent carbons is small, the three shielding components for each carbon may be obtained from the analyses of the powder pattern of the stationary sample or the spinning sidebands (SSB) in MAS spectroscopy in the crystalline phase. However, as shown in the upper 1-D spectrum of Figure 8, the SSB patterns are complex due to overlap among many inequivalent carbons. We therefore resorted to the 2-D TOSS-deTOSS technique by

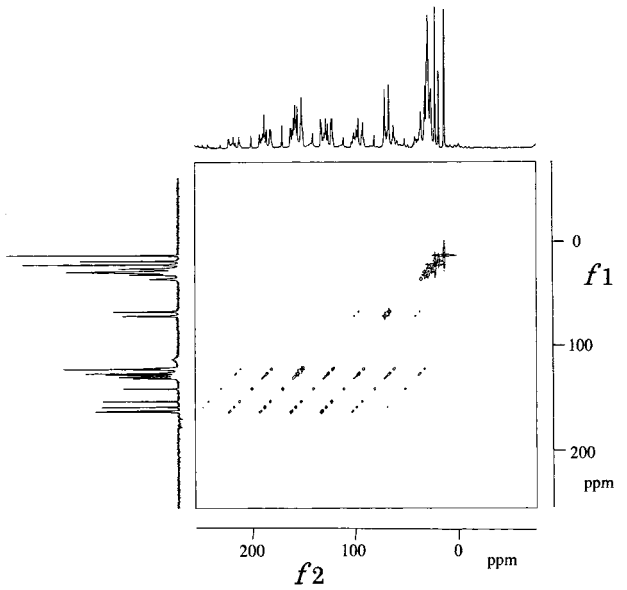

Figure 8. 2-D site-separated spinning sideband spectrum of MHPOBC in the solid state. The horizontal (f_2) axis spectrum is the usual MAS spectrum with complex SSB patterns, while the vertical (f_1) axis spectrum is a sideband-free isotropic shielding spectrum.

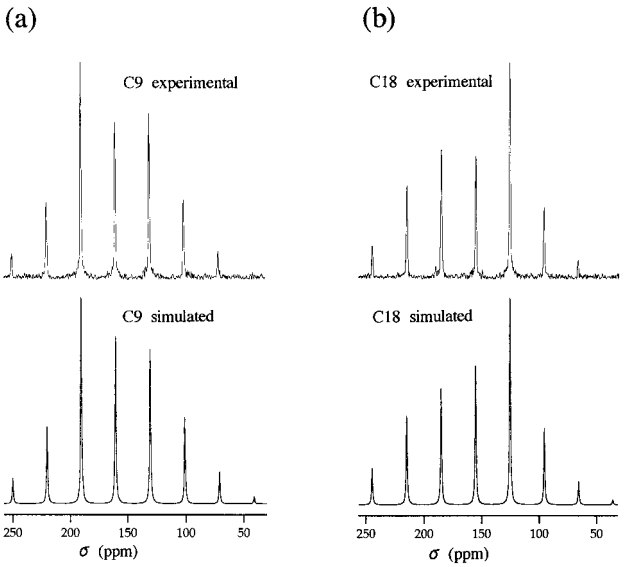

Figure 9. Site-selected spinning sideband patterns and simulated spectra for C(9) and C(18). Results of simulation are summarized in Table 4.

Kolbert and Griffin,[7] where SSB are resolved according to the isotropic shielding values of the respective nuclei by applying sample rotation−synchronized π-pulses, TOSS (total suppression of SSB) sequence,[15] to eliminate SSB in the t_1 evolution period and collecting the free decay signal without eliminating SSB (deTOSS) in the t_2 detection period. Then the spectrum in the f_2 dimension consists of the usual complex SSB patterns while the spectrum in the f_1 dimension is an SSB-free isotropic shielding pattern, as shown in Figure 8. The 2-D contour plot, when sliced at a certain σ_{iso} value, gives an SSB pattern for each carbon atom.

Figure 9 shows examples of this site-separated SSB patterns for C(9) and C(18). They both are aromatic nonprotonated carbons attached to oxygen and would possess similar electronic structure: $\sigma_{iso}(j)$ values differ by only 5.4 ppm, but the site-separated SSB patterns reveal the remarkable difference in $\sigma^{j-PAS}(j)$ tensors. Comparison with simulated spectra[16] in Figure 9 revealed tensor principal values of 244.1, 169.3, and 67.8 ppm with $\sigma_{iso}(9) = 160.0$ ppm for C(9) and 255.9, 137.4, and 71.7 ppm with $\sigma_{iso}(18) = 155.5$ ppm for C(18).

TABLE 4: Shielding Tensor Components Determined by 2-D Site-Separated Spinning Sideband Spectroscopy

j	f	types	σ_{xx}^{j-PAS} (ppm)	σ_{yy}^{j-PAS} (ppm)	σ_{zz}^{j-PAS} (ppm)	σ_{iso} (ppm)	RMS[a]	# of SSB simulated
9	*b*1	CC	244.1	169.3	67.8	160.4	3.4556	9
11	*b*1	CH	217.9	145.5	21.8	128.4	2.8618	9
13	*b*2	CC	236.0	173.0	20.0	143.0	2.9014	9
14	*b*2	CH	200.8	150.2	21.3	124.1	2.9938	9
17	*bc*	CO	255.9	118.1	118.0	164.0	1.6687	7
18	*p*	CC	255.9	137.4	71.7	155.0	4.6781	7
22	*pc*	CO	257.5	139.0	98.2	164.9	6.8271	6

[a] RMS $= \sqrt{(1/n)\sum_{k=1}^{n}[I^{exptl}(j;k)-I^{calcd}(j;k)]^2}$, where $I^{exptl}(j;k)$ and $I^{calcd}(j;k)$ are, respectively, the kth SSB intensities of the jth carbons and n is the number of SSB used for simulation. A series of $I^{exptl}(j;k)$ ($k = 1, 2, ..., n$) are normalized such that the maximum intensity is 100 for each carbon.

In this way we could obtain the principal components with enough reliability for seven carbons for which the resonance lines are well resolved in the crystalline phase, and they are summarized in Table 4. The root-mean-square (RMS) of the deviation between the simulated and experimental spectra and the number of SSB used for the RMS estimate are also shown.

V.2. Rigid Core Model. To analyze orientational order by using the experimentally obtained shielding tensor, a model treatment is necessary for intramolecular motions, namely, the quantities $\langle\ \rangle$ in eq 14 should be evaluated as averages specific to the motional modes: In the present paper, we attempt to determine the order parameter S_{00} and the orientations of the fragments given by the angles such as β_b and β_p for MHPOBC at 403 K in the S_A phase. The S_A phase is a uniaxial phase without tilt ($\theta_0 = 0$). The molecular biaxiality is believed to be small in the high-temperature region, such as in the present case, and therefore is neglected. The phase and molecular biaxialities and the tilt of the director from the external magnetic field will be important in the lower temperature phases, S_{CA}* and so forth.

To start with, we use the rigid core model where the five fragments are fixed on the MOL frame and no internal motions are present in the core part. $\langle\sigma_{zz}^{LAB}(j)\rangle$ in this model is calculated by eliminating the angular brackets $\langle\ \rangle$ in eq 14 and by taking the angular factors $\gamma_j + \alpha_f$ into account explicitly. This model gives a characteristic feature to the NMR spectrum and allows the two aromatic protonated carbons at the same j position to be distinguished. If we designate the two carbons j and j' as shown in Figure 3, the two atoms are distinguished by their third Eulerian angles, $\gamma_j = 0$ and $\gamma_{j'} = \pi$. By putting them into eq 14, the spectral difference is derived as

$$\Delta\langle\sigma_{zz}^{LAB}(j',j)\rangle \equiv \langle\sigma_{zz}^{LAB}(j')\rangle - \langle\sigma_{zz}^{LAB}(j)\rangle$$
$$= [\sigma_{xx}^{j-PAS}(j) - \sigma_{yy}^{j-PAS}(j)]\sin 2\alpha_j \sin \alpha_f \sin 2\beta_f S_{00} \quad (18)$$

and are given, for example, by

$$\Delta\langle\sigma_{zz}^{LAB}(11',11)\rangle = 61.92 \sin \alpha_{b1} \sin 2\beta_b S_{00} \text{ ppm} \quad (19)$$

and

$$\Delta\langle\sigma_{zz}^{LAB}(14',14)\rangle = 43.82 \sin \alpha_{b2} \sin 2\beta_b S_{00} \text{ ppm} \quad (20)$$

If we take $\beta_b = 5-10°$ and $S_{00} = 0.7-0.8$, then the spectral differences are (7.53 sin α_{b1}) ppm and (5.33 sin α_{b2}) ppm for $j = 11$ and 14, respectively. Our experiment, on the other hand,

TABLE 5: Numerical Results for the Free Internal Rotation Model

β_b	7.3°	α_{17}	30.2°
β_p	−8.0°	α_{22}	30.9°
S_{00}	0.73		

shows, in Figure 4b, that these NMR lines are fairly narrow, requiring that $|\Delta\langle\sigma_{zz}^{\mathrm{LAB}}(j,j')\rangle|(j = 11,14)$ must be less than 0.1 ppm. This requires both α_{b1} and α_{b2} to be less than 1°, meaning that all three phenylene rings lie almost exactly in the same plane on which the y^{MOL} axis lies. This restriction is too strict and is almost unrealistic. One therefore must change the model in which some intramolecular motion averages out the inequivalences of j and j' for the protonated ring carbons.

V.3. Free Rotation Model. The simplest way with which the intramolecular motion is taken into account is to assume free rotation for all the segments discussed in section III, i.e., to use eq 15 with $P_2(\cos\theta_0) = 1$. For aromatic carbons the Eulerian angles related with j-PAS → f-FRAG transformations take definite values given in Table 1, and therefore one can apply eq 15 to four carbons, C(9), C(11), C(13), and C(14), of the biphenylene core and to C(18) of the phenylene core, among the seven carbons for which the shielding tensor elements were determined experimentally. Then the values of $P_2(\cos\beta_b)S_{00}$ are obtained: 0.7455 for C(9), 0.6960 for C(11), 0.7667 for C(13), and 0.6323 for C(14). Taking an average

$$P_2(\cos\beta_b)S_{00} = 0.7101 \tag{21}$$

resulted. The experimental result for C(18) gave

$$P_2(\cos\beta_p)S_{00} = 0.7066 \tag{22}$$

for the phenylene core. The two values are close, and this result relieves the difficulty in the rough approximation given in section IV.4.

The j-PAS → f-FRAG Eulerian angles for the ester linkages, especially α_j, are generally dependent on the local electronic structure. The values of α_j were determined from the experimental data using eq 15 and the $P_2(\cos\beta_f)$ values obtained above. The angles thus determined, $\alpha_{17} = 30.7°$and $\alpha_{22} = 30.9°$, are very plausible, meaning that the second shielding axis ($y^{j-\mathrm{PAS}}$, $j = 17$ or 22) points nearly parallel to the C═O double bond.

To determine β_b, β_p, and S_{00}, another restraint is necessary. We employ an X-ray structure report[17] that the two core axes ($z^{b1-\mathrm{FRAG}}$ or $z^{b2-\mathrm{FRAG}}$ and $z^{p-\mathrm{FRAG}}$) make an angle of 15.3°. By assuming

$$|\beta_b - \beta_p| = 15.3° \tag{23}$$

in liquid crystal, too, and solving with eqs 18 and 19, the parameters were determined uniquely: $\beta_b = 7.3°$, $\beta_p = -8.1°$, and $S_{00} = 0.73$. The results for the free rotation model are summarized in Table 5. All results are reasonable, and therefore, the free rotation model seems successful.

We may point out, however, the limitations of this simple model. First, $P_2(\cos\beta_b)S_{00}$ evaluated for each carbon scatters. It is noteworthy that 0.6960 and 0.6323 obtained for the protonated carbons are significantly smaller than 0.7455 and 0.7667 obtained for the nonprotonated carbons. This probably comes from the oversimplified model for internal rotation. Second, the free internal rotation model seems unrealistic because the π-orbital overlap across the fragments stabilizes the electronic energy, and therefore, the rotation about the single bonds connecting the fragments may be restricted. In the next section we treat a model with restricted motions.

V.4. Ring Flip Model. Ring flip motions by which the aromatic ring takes two stable rotational isomeric positions characterized by $\alpha_f = \alpha_{f0}$ and $\alpha_{f0} + \pi$ is an attractive model because it averages out the spectral difference between jth and j'th protonated carbons, $\Delta\langle\sigma_{zz}^{\mathrm{LAB}}(j',j)\rangle$ defined in eq 18, by

$$\langle\sin(\gamma_j + \alpha_f)\rangle = 0 \tag{24}$$

and

$$\langle\cos 2(\gamma_j + \alpha_f)\rangle = \cos 2\alpha_{f0} \tag{25}$$

and also because it guarantees the interfragmental π-conjugation. $\mathrm{AIS}^{\mathrm{flip}}(j)$ for the protonated carbons are

$$\mathrm{AIS}^{\mathrm{flip}}(j,\ \text{protonated}) = \frac{1}{2}[\sigma_{zz}^{j-\mathrm{PAS}}(j) - \sigma_{\mathrm{iso}}(j)] \times \left[-P_2(\cos\beta_f) + \frac{3}{2}\cos 2\alpha_{f0}\sin^2\beta_f\right]S_{00} - \frac{1}{4}[\sigma_{xx}^{j-\mathrm{PAS}}(j) - \sigma_{yy}^{j-\mathrm{PAS}}(j)]\left[P_2(\cos\beta_f) + \frac{1}{2}\cos 2\alpha_{f0}\sin^2\beta_f\right]S_{00} \tag{26}$$

On the other hand, the flip motion does not affect the spectra of aromatic nonprotonated carbons. Considering that $\alpha_j = \gamma_j = 0$ for these carbons

$$\mathrm{AIS}^{\mathrm{flip}}(j,\ \text{nonprotonated}) = \frac{1}{2}[\sigma_{zz}^{j-\mathrm{PAS}}(j) - \sigma_{\mathrm{iso}}(j)] \times \left[-P_2(\cos\beta_f) + \frac{3}{2}\cos 2\alpha_{f0}\sin^2\beta_f\right]S_{00} + \frac{1}{2}[\sigma_{xx}^{j-\mathrm{PAS}}(j) - \sigma_{yy}^{j-\mathrm{PAS}}(j)]\left[P_2(\cos\beta_f) + \frac{1}{2}\cos 2\alpha_{f0}\sin^2\beta_f\right]S_{00} \tag{27}$$

is obtained. The difference in coefficients of the second terms acts to improve the scattering of the numerical results found for the free rotation model. However, the calculations have not given a satisfactory result until now. This may be partly related to the neglect of molecular biaxiality. The analysis taking this aspect into account and also the analysis for the biaxial phases at lower temperature are now in progress.

In conclusion, the free internal rotation model is satisfactory as long as the effective symmetry of the whole molecule (MRB) is regarded as a symmetric top. More rigorous treatment for internal rotation will be necessary if one takes into account the molecular biaxiality.

Acknowledgment. We thank Atsuo Fukuda, Hideo Takezoe, and Yoichi Takanishi for offering the samples and for valuable discussions. Jean-Pierre Bayle is acknowledged for advice on spectral assignment.

References and Notes

(1) Chandani, A. D. L.; Gorecka, E.; Ouchi, Y.; Takezoe, H.; Fukuda, A. *Jpn. J. Appl. Phys.* **1989**, *28*, L1265.

(2) Fukuda, A.; Takanishi, Y.; Isozaki, T.; Ishikawa, K.; Takezoe, H. *J. Mater. Chem.* **1994**, *4*, 997.

(3) Suzuki, Y.; Hagiwara, T.; Kawamura, I.; Okamura, N.; Kitazume, T.; Kakimoto, M.; Imai, Y.; Ouchi, Y.; Takezoe, H.; Fukuda, A. *Liq. Cryst.* **1989**, *6*, 167.

(4) Nakai, T.; Miyajima, S.; Takanishi, Y.; Yoshida, S.; Fukuda, A. *J. Phys. Chem. B* **1999**, *103*, 406.

(5) Asahina, S.; Sorai, M.; Fukuda, A.; Takezoe, H.; Furukawa, K.; Terashima, K.; Suzuki, Y.; Kawamura, I. *Liq. Cryst.* **1997**, *23*, 339.

(6) (a) Bax, A.; Freeman, R.; Kempsell, S. P. *J. Am. Chem. Soc*. **1980**, *102*, 4849. (b) Bax, A.; Freeman, R.; Frenkiel, T. A. *J. Am. Chem. Soc*. **1981**, *103*, 2102.

(7) Kolbert, A. C.; Griffin, R. G. *Chem. Phys. Lett*. **1990**, *166*, 87.

(8) Mehring, M. *Principles of High-Resolution NMR in Solids*, 2nd ed.; Springer-Verlag: Berlin, 1983.

(9) (a) Duncan, T. M. *J. Phys. Chem. Ref. Data* **1987**, *16*, 125. (b) Veeman, W. S. *Prog. Nucl. Magn. Reson. Spectrosc*. **1984**, *16*, 193.

(10) (a) Maier, W.; Saupe, A. *Z. Naturforsch*. **1959**, *14a*, 882. (b) Maier, W.; Saupe, A. *Z. Naturforsch*. **1960**, *15a*, 287.

(11) Emsley, J. W. *Nuclear Magnetic Resonance of Liquid Crystals*; Reidel: Dordrecht, 1985.

(12) The C(21)−C(22) coherence peak was detected, although this connection is similar to C(16)−C(17) in that these are aromatic nonprotonated carbonyl pairs. We have no definite explanation for the difference between these pairs on the 2-D INADEQUATE spectrum. One possibility is that the spin−lattice relaxation time of C(17) is longer than that of C(22). We observed different relaxation behaviors for the two carbonyl carbons, namely, the activation energy for C(17) is larger than that of C(22) in the S_A phase. The relaxation study is reported in Tokumaru, K.; Jin, B.; Yoshida, S.; Takanishi, Y.; Ishikawa, K.; Takezoe, H.; Fukuda, A.; Nakai, T.; Miyajima, S. *Jpn. J. Appl. Phys*. **1999**, *38*, 255.

(13) Pretsch, E.; Clerc, T.; Seibl, J.; Simon, W. *Tables of Spectral Data for Determination of Organic Compounds*; Springer: Berlin, 1989.

(14) Luzar, M.; Rutar, V.; Seliger, J.; Blinc, R. *Ferroelectrics* **1984**, *58*, 115.

(15) Dixon, W. T. *J. Chem. Phys*. **1982**, *77*, 1800.

(16) Herzfeld, J.; Berger, A. E. *J. Chem. Phys*. **1980**, *73*, 6021.

(17) Hori, K.; Endo, K. *Bull. Chem. Soc. Jpn.* **1993**, *66*, 46.